



# OPEN PTPN2 inhibits TG-induced ERS-initiated TNBC apoptosis through the mitochondrial pathway

Yanhe An<sup>1</sup>, Jinxin Lan<sup>1</sup>, Jiaping Tang<sup>1,2</sup> & Na Luo<sup>1</sup>✉

Triple negative breast cancer (TNBC) is the most malignant subtype of breast cancer that portends a poor prognosis and limited treatment. PTPN2 is a member of the non-receptor protein tyrosine phosphatase family that regulates biological processes by dephosphorylating various signaling molecules. Endoplasmic reticulum stress (ERS) plays a dual regulatory role by promoting both survival and apoptosis. This study aims to elucidate the role of PTPN2 in mediating the pro-apoptotic effects of ERS induced by Thapsigargin (TG), and its influence on the fate of TNBC cells, utilizing both loss-of-function and gain-of-function methodologies. Our findings indicate that PTPN2 modulates TG-induced ERS via the IRE1-XBP1 and PERK/EIF2 $\alpha$ /ATF-4 signaling pathways. Furthermore, PTPN2 mitigates the TG-induced reduction in cell proliferation and the concomitant increase in apoptosis. Specifically, PTPN2 appears to inhibit several facets of TG-induced apoptosis, including: (1) Ca<sup>2+</sup> elevation in mitochondria, (2) the production of reactive oxygen species (ROS), and (3) Bax/Bcl-2 augmentation which dictates mitochondria-mediated apoptosis. Additionally, we observed that the knockdown of PTPN2 enhances TG-induced autophagy; however, our results suggest that autophagy may serve a protective role against TG-induced apoptosis. Consequently, targeting PTPN2 in conjunction with ERS-inducing agents may represent a promising therapeutic strategy for the treatment of TNBC.

**Keywords** PTPN2, ERS, Apoptosis, The mitochondrial pathway, TNBC

Breast cancer is the most frequently diagnosed malignancy and the second leading cause of cancer-related mortality among women globally<sup>1</sup>. Triple-negative breast cancer (TNBC) constitutes approximately 15% to 20% of all breast cancer subtypes and is characterized by the absence of estrogen receptors, progesterone receptors, and human epidermal growth factor receptor 2<sup>2,3</sup>. Compared to other breast cancer subtypes, TNBC is associated with a heightened level of invasiveness, a higher recurrence rate, and a poorer prognosis<sup>4</sup>. Patients diagnosed with TNBC do not respond to targeted endocrine or receptor therapies due to the absence of the aforementioned receptors. Currently, the standard treatment modalities for TNBC include surgical resection and non-specific chemotherapy<sup>5,6</sup>. Recently, immune checkpoint inhibitors (ICIs) have been introduced as a treatment option for TNBC; however, the clinical benefits observed have been less than promising<sup>7</sup>. Therefore, there is a pressing need for the development of more effective therapeutic strategies for TNBC.

The endoplasmic reticulum (ER) is integral to various cellular processes, including protein synthesis and folding, lipid synthesis and distribution, as well as calcium ion (Ca<sup>2+</sup>) storage and release, among other functions<sup>8,9</sup>. Disruption of ER homeostasis can occur due to fluctuations in ATP levels, variations in Ca<sup>2+</sup> concentrations, hypoxic conditions, viral infections, the presence of inflammatory cytokines, nutrient deprivation, and exposure to environmental toxins, all of which can lead to the accumulation of misfolded proteins<sup>10</sup>. In order to maintain ER homeostasis and alleviate endoplasmic reticulum stress (ERS), activation of the unfolded protein response (UPR) occurs<sup>11</sup>. The UPR consists of three primary signaling pathways: inositol-requiring enzyme 1 (IRE1), PKR-like ER kinase (PERK), and activating transcription factor 6 (ATF6). Furthermore, the ER chaperone binding immunoglobulin protein (BiP) is crucial for sensing ER stress. Under normal physiological conditions, BiP interacts with ER stress sensors, keeping them in an inactive state. However, during ER stress, BiP binds to unfolded or misfolded proteins within the ER, which results in the release of IRE1 $\alpha$  and PERK, facilitating their homodimerization, as well as the translocation of ATF6 to the Golgi apparatus<sup>12,13</sup>. IRE1 $\alpha$  is responsible for the splicing of XBP1 mRNA, which encodes a significant transcription factor that activates the expression of genes associated with the UPR that are crucial for endoplasmic reticulum (ER) proteostasis and cellular pathophysiology. The protein kinase PERK phosphorylates the eukaryotic translation initiation factor 2

<sup>1</sup>Department of Anatomy and Histology, School of Medicine, Nankai University, 94 Weijin Road, Tianjin 300071, China. <sup>2</sup>Life Science Research Center, The First Affiliated Hospital of Xinxiang Medical University, Weihui 453100, Henan, China. ✉email: luon11@nankai.edu.cn

subunit- $\alpha$  (EIF2 $\alpha$ ), thereby facilitating the translation of ATF4. This transcription factor subsequently activates the expression of UPR target genes that encode proteins involved in amino acid biosynthesis, the antioxidative response, autophagy, and apoptosis. Additionally, ATF6 translocates from the ER to the Golgi apparatus, resulting in the production of an active cytosolic fragment of ATF6, which also promotes the transcription of UPR target genes that are essential for maintaining ER protein folding homeostasis and overall cellular physiology<sup>13</sup>. UPR plays a dual role. Firstly, the UPR restores ER homeostasis, promotes correct protein folding, induces autophagy, and promotes cell survival under mild ERS conditions. Secondly, the UPR induces mitochondrial apoptosis under severe ERS condition<sup>14,15</sup>. Consequently, a comprehensive understanding of the ERS pathway and the mechanisms leading to apoptosis may provide valuable insights for developing effective clinical strategies for the treatment of TNBC.

Protein tyrosine phosphatase non-receptor type 2 (PTPN2), commonly referred to as T-cell protein tyrosine phosphatase (TCPTP), is a widely expressed enzyme that functions as a tyrosine phosphatase. In humans, it predominantly exists in two isoforms: the 48-kDa variant (TC48), which is localized to the endoplasmic reticulum due to a hydrophobic C-terminal region, and the 45-kDa variant (TC45), which is targeted to the nucleus through a C-terminal nuclear localization sequence<sup>16</sup>. PTPN2 plays a critical role in regulating numerous biological processes by dephosphorylating and inactivating various substrate proteins, including members of the Src family kinase<sup>17</sup>, epidermal growth factor receptor (EGFR)<sup>18</sup>, vascular endothelial growth factor (VEGFR)<sup>19</sup>, Janus kinase 1 and 3 (JAK1, JAK3), and signal transducer and activator of transcription 1 and 3 (STAT1, STAT3)<sup>20</sup>. PTPN2 has garnered significant interest due to its role in enhancing the sensitivity of tumor cells to immunotherapy and improving the overall efficacy of such treatments<sup>21–23</sup>. In this context, efforts are currently being made to develop specific small molecule inhibitors targeting PTPN2<sup>24–26</sup>. It is important to note, however, that the influence of PTPN2 on tumor proliferation is contingent upon the effects mediated by interferon- $\gamma$ , rather than through direct suppression of tumor cell growth. Consequently, investigating strategies that could leverage the additive effects of PTPN2, in addition to its interferon- $\gamma$ -mediated actions on tumor growth, presents a promising avenue for further research.

In this research, we examined the function of PTPN2 in the ERS process and its impact on the progression of TNBC utilizing both loss-of-function and gain-of-function methodologies. Our findings indicate that PTPN2 participates in TG-induced ERS by activating the IRE1-XBP1 and PERK/EIF2 $\alpha$ /ATF-4 signaling pathways. Additionally, we observed that autophagy serves a protective role against TG-induced apoptosis. Consequently, we propose that targeting PTPN2 in combination with ERS-inducing agents may represent a promising therapeutic approach for the treatment of TNBC.

## Materials and methods

### Cell culture and treatment

Human embryonic kidney 293T (HEK-293T), human breast cancer cell lines MDA-MB-231 and SUM159 were obtained from the National Collection of Authenticated Cell Cultures, and cultured in DMEM medium (VivaCell) supplemented with 10% fetal bovine serum (VivaCell) and 100U/ml penicillin–streptomycin (VivaCell) at 37 °C in a humidified incubator with 5% CO<sub>2</sub>. Murine breast cancer cell line 4T1 was cultured in RPMI 1640 medium (VivaCell) supplemented with 10% fetal bovine serum (VivaCell) and 100U/ml penicillin–streptomycin (VivaCell) at 37 °C in a humidified incubator with 5% CO<sub>2</sub>.

When necessary, 10  $\mu$ M MG132 (MCE) was added medium for indicated time to inhibit protein degradation. 1  $\mu$ M thapsigargin (TG, MCE) or 5  $\mu$ g/mL tunicamycin (TM, GLP BIO) was added medium for 48 h to induce ERS. And 20  $\mu$ M chloroquine (CQ, MCE) was added medium for 2 h to inhibit autophagy.

### Vector construction and establishment of stable cell lines

For gene overexpression, DNA sequences encoding the human PTPN2-45KD, PTPN2-48KD were amplified using polymerase chain reaction (PCR)-amplified from MDA-MD-231 cDNA and subsequently cloned into the pLV-EF1 $\alpha$ -MCS-IRES-Bsd plasmid (Biosettia, San Diego, CA). For gene silencing, short hairpin RNAs (shRNAs) targeting human PTPN2 were cloned into the pLV-H1-EF1 $\alpha$ -puro plasmid (Biosettia). The lentiviruses carrying the overexpression vectors, gene silencing vectors, or empty vectors were conducted in accordance with according to the manufacturer's instruction. Lentivirus-containing medium was applied to cells in the presence of 8  $\mu$ g/ml polybrene (Sigma-Aldrich) for 48 h, prior to selection with 10  $\mu$ g/ml blasticidin (Sigma-Aldrich) or 1  $\mu$ g/ml puromycin (Sigma-Aldrich) for one week to establish stable cell lines. The primers and shRNAs are listed in Table S1, and the PTPN2 cDNA (NM\_002828.4 and NM\_080422.3) sequence is in the Supporting Information.

### Western blot

Twenty micrograms of protein isolated from MDA-MB-231 and SUM159 cells was loaded to 10% sodium dodecyl sulfate–polyacrylamide gel for electrophoresis. The protein was then transferred to a polyvinylidene fluoride membrane. After blocking with 5% nonfat milk, the membrane was incubated with a primary antibody to either of the following: GRP78 (200,310-4F11, Zenbio), IRE1 (220,399, Zenbio), XBP1 (R27438, Zenbio), CHOP (WL00880, Wanleibio), PERK (WL03378, Wanleibio), P-PERK (WL05295, Wanleibio), P-EIF2 $\alpha$  (ET1603-14, HuaBio), P-IRE1 (HA721980, HuaBio), Ki67 (ET1609-34, HuaBio), LC3 (ET1701-65, HuaBio), p62 (HA721171, HuaBio), ATF-6 (24,169-1-AP, Proteintech), PTPN2 (11,214-1-AP, Proteintech), GAPDH (60,004-1-Ig, Proteintech), Bcl-2 (26,593-1-AP, Proteintech), TCPTP (58935S, CST), Ubiquitin (3936S, CST), cleaved Caspase 3 (9664T, CST), Bax (2772T, CST), AMPK (5831S, CST) and P-AMPK (2535S, CST) overnight at 4 °C. The membrane was exposed to chemiluminescence (Thermo Fisher Scientific, USA) after incubation with corresponding secondary antibodies to detect specific signals.

### Co-Immunoprecipitation

Cells were lysed in buffer A (50 mM Tris/HCl, pH7.5, 150 mM NaCl, 1 mM EDTA, 1 mM EGTA, 25 mM NaF, 5 mM NaP<sub>2</sub>O<sub>7</sub>, 1% TritonX-100, 1 mM Na<sub>3</sub>VO<sub>4</sub>, 20 mM p-nitrophenyl phosphate, 2 µg/ml leupeptin, 2 µg/ml aprotinin and 100 µg/ml PMSF) and protein concentrations were determined using the BCA Protein Assay Kit (Beyotime). Briefly, precleared cell lysate supernatants were incubated with anti-IgG (sc-2025, Santa Cruz) or anti-FLAG (BAO3183103, Bioss). The immunocomplexes were collected with Dynabeads™ protein G and immunoblotting was performed to detect expression of FLAG and GRP78.

### Quantitative real time PCR

Total RNA was extracted using Trizol according to manufacturer's instructions. EasyScript® First-Strand cDNA Synthesis SuperMix (TransGen, #AE301-02) was used to synthesise complementary DNA (cDNA). RT-PCR was performed with a Bio-Rad CFX machine (Bio-Rad Laboratories, Hercules, CA) and SYBR Green reagent (YEASEN, #11184ES03). Relative quantitation of target gene expression was measured by the  $2^{-\Delta\Delta C_t}$  method and GAPDH was deemed as a reference. The primer sequences are in Table S1.

### Nuclear Hoechst33342 staining

Cells were stained with 5 µg/ml Hoechst 33,342 for 30 min in the dark. Subsequently, photomicrographs were taken with an OlympusBX51 fluorescence microscope (Olympus, Tokyo, Japan).

### EdU staining

Cell proliferation was examined using the Edu A488 detection kit (Beyotime, #C0071S) and performed according to manufacturer's instructions. Briefly, Incubate the cells with 10 µM EdU staining solution for 10–20 min in the dark. Subsequently, photomicrographs were taken with an OlympusBX51 fluorescence microscope (Olympus, Tokyo, Japan).

### Live/dead cell viability assay

Live/ Dead cell viability assay was performed according to the manufacturer's protocol. In brief, cells stained with Calcein-AM/EthD1 (Thermo Scientific, # L3224) for 30 min at 37 °C. At last, cells were promptly imaged under inverted fluorescence microscope. Subsequently, photomicrographs were taken with an OlympusBX51 fluorescence microscope (Olympus, Tokyo, Japan).

### Immunohistochemistry (IHC)

The murine 4T1 ex vivo tumor tissues were incubated with anti-Ki67, anti-cleaved Caspase 3, and CHOP antibodies at 4 °C overnight. The tissue sections were then incubated with a secondary antibody followed by peroxidase-anti-peroxidase (PAP) complex. The tissue sections were then incubated in a diaminobenzidine (DAB)/ hydrogen peroxide substrate solution to obtain a brown reaction product. The tissue sections were counterstained with hematoxylin. Ki67 and cleaved caspase3 in the murine 4T1 ex vivo tumor tissues were scored according to positive cells of 3 sections. CHOP in the murine 4T1 ex vivo tumor tissues were scored according to IDO (integrated option density/area) of 3 sections. Photomicrographs were taken with an OlympusBX51 fluorescence microscope (Olympus, Tokyo, Japan). Ki67 and cleaved Caspase3 in the murine 4T1 ex vivo tumor tissues were scored according to percentage of positive cells in 3 sections. And Image J software was used to assess the Average Optical Density of CHOP IHC images.

### Ex vivo culture

The mice needed for the experiment were purchased from Beijing Vital River Laboratory Animal Technology Co. Ltd. Animal studies were approved by the Animal Care and Use Committee of the Nankai University. Five-week-old female BALB/ c mice were inoculated with  $1 \times 10^5$  4T1sgGFP or sgPTPN2 cells to the 4th pair of fat pads, respectively. Mice were humanely euthanized when tumor volume reached 500–600 mm<sup>3</sup> via isoflurane inhalation followed by rapid cervical dislocation, and the tumors were separated from the mice and cut into 1–2 mm<sup>3</sup> blocks in a sterile environment. The blocks were cultured with RPMI1640 supplemented with 10% fetal bovine serum and 1X antibiotic/ antimycotic with the presence of DMSO or 1 µM TG for 24 h, and embedded in paraffin for immunohistochemistry staining or snap freeze for WB. We confirm that all methods were performed in accordance with the relevant guidelines and regulations.

### Annexin V/Propidium iodine (PI) staining

Apoptosis was detected by an Annexin V-FITC/PI Apoptosis Detection Kit (Simu Biotech, #A5001-02P-L). The cells were washed with cold PBS and resuspended in Annexin V-binding buffer at a concentration of  $1 \times 10^6$ /ml. The suspension was incubated with Annexin V-FITC and PI for 15 min at room temperature in the dark. After adding binding buffer to each tube, the cells were analyzed by flow cytometry.

### Detection of ROS generation

The cells were incubated with 2', 7'-dichlorofluorescein diacetate (DCFH-DA, Beyotime, #S0033S) at 37 °C for 40 min according to the manufacturer's instructions. Subsequently, photomicrographs were taken with an OlympusBX51 fluorescence microscope (Olympus, Tokyo, Japan).

### Detection of mitochondrial calcium concentration

Cells were seeded on a 15 mm Confocal Dish and incubated for 24 h. Then they were incubated with the indication TG concentration for 48 h. After removing the medium, the cells were washed three times with serum-free medium. The cells were first stained with 1 µM Mito-Tracker Green for at 37 °C 40 min, followed by

4  $\mu$ M Rhod2-AM staining at 4 °C for 1 h in the dark. photomicrographs were taken with an Olympus FV1000 confocal microscope equipped with a 100 $\times$  oil immersion objective. (Olympus, Tokyo, Japan).

# Statistical analysis

Data analysis was performed using GraphPad Prism software. All assays were performed in triplicate, and at least 3 independent experiments were conducted per test series. Student's *t*-test was used to compare the significance between the two sets of data. One-way ANOVA is used for data comparison between multiple groups. The results are presented as the mean  $\pm$  standard deviation (SD). A *p* value < 0.05 was considered statistically significant.

# Results

## PTPN2 regulates the occurrence of ERS in TNBC

Our previous studies indicated that the overexpression of PTPN2 (45 kDa and 48 kDa) leads to a reduction in ubiquitin expression, while the knockdown of PTPN2 results in an increase in ubiquitin expression in a time-dependent manner in MDA-MB-231 cells treated with MG132 (a proteasome inhibitor) (Supplementary Fig. 1). These results suggest that PTPN2 plays a role in the protein degradation pathway in TNBC cells. An imbalance between protein synthesis and protein degradation disrupts proteostasis followed by ERS activation. Utilizing co-immunoprecipitation (Co-IP), we identified an interaction between PTPN2 and GRP78, a marker protein for ERS, in MDA-MB-231 cells, indicating a direct protein–protein interaction (Fig. 1A). Moreover, in order to determine whether PTPN2 regulates ERS activation, we treated PTPN2 over-expression and PTPN2 knockdown MDA-MB-231 and SUM159 cells with thapsigargin (TG; an ERS-inducing agent). We found that PTPN2 (45 kDa and 48 kDa) over-expression decreases GRP78 expression in TG-treated MDA-MB-231 and SUM159 cells (Fig. 1B), whereas PTPN2 knockdown results in an increase in GRP78 expression in these same cell lines under TG treatment (Fig. 1C).

## PTPN2 inhibits TG-induced ERS through IRE1-XBP1 and PERK/EIF2 $\alpha$ /ATF-4 pathways

In light of the role of PTPN2 in ERS regulation, we first examined mRNA expression of several key molecules in the UPR signaling pathway in MDA-MB-231 and SUM159 cells using qPCR. Our results showed that PTPN2 (45 kDa and 48 kDa) over-expression not only significantly inhibits mRNA expression of IRE1, XBP1, ATF-4 and ATF-6 but also shows a trend towards inhibition of GRP78 mRNA expression in DMSO-treated MDA-MB-231 cells.

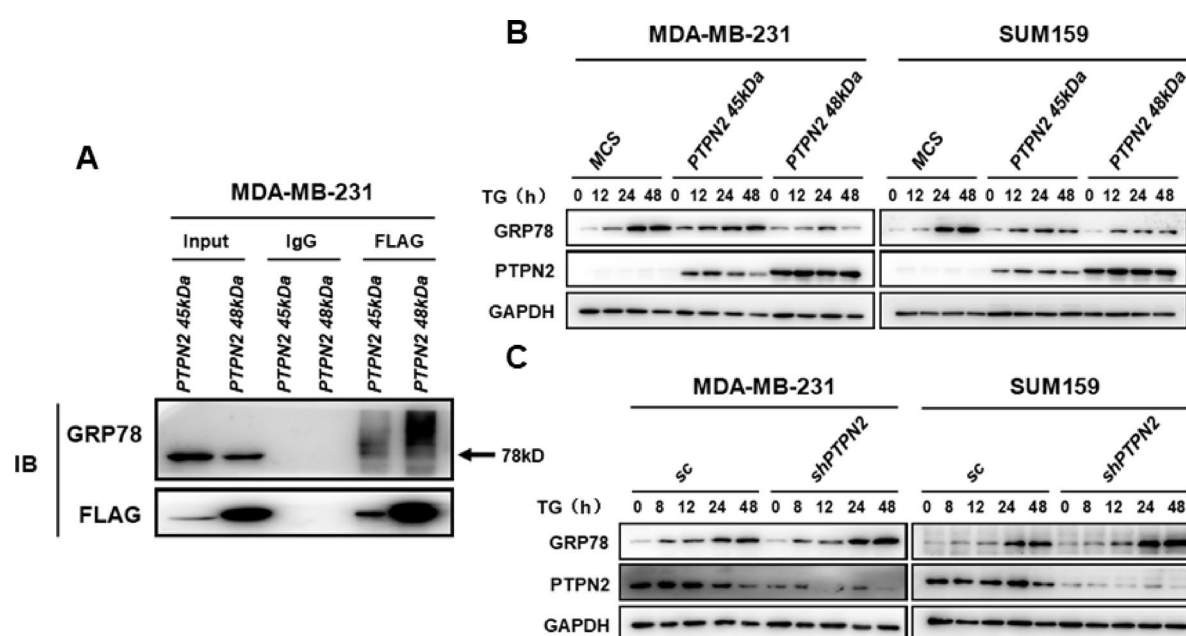


**Fig. 1.** PTPN2 directly interacts with and inhibits GRP78 in TNBC. (A) The Western blot shows a direct interaction of PTPN2 45 kDa or PTPN2 48 kDa with GRP78. The protein lysate was precipitated with anti-IgG or anti-Flag, and blot with anti-GRP78 or anti-Flag. Input: whole cell lysate; IgG: negative control; Flag: representing PTPN2 45 kDa or PTPN2 48 kDa. (B) The Western blot shows ectopic expression of PTPN2 45 kDa or PTPN2 48 kDa diminishes GRP78 expression in TG-treated MDA-MB-231 and SUM159 cells, most obviously at 48 h. PTPN2 serves to indicate over-expression of PTPN2, and GAPDH serves as a loading control. All experiments are conducted as a single independent experiment (*n* = 1). (C) The Western blot shows knockdown of PTPN2 augments GRP78 expression in TG-treated MDA-MB-231 and SUM159 cells, most obviously at 48 h. PTPN2 serves to indicate knockdown of PTPN2, and GAPDH serves as a loading control. All experiments are conducted as a single independent experiment (*n* = 1).



In addition, we found that PTPN2 (45 kDa and 48 kDa) over-expression significantly inhibits mRNA expression of GRP78, IRE1, XBP1, and ATF-4 while PTPN2 (45 kDa) over-expression alone significantly inhibits mRNA expression of ATF-6 in TG-treated MDA-MB-231 cells. SUM159 cells demonstrate a similar mRNA expression pattern as observed in MDA-MB-231 cells in regard to key molecules in the UPR signaling pathway (Fig. 2A,B). We then examined the protein expression of several key molecules in the UPR signaling pathway using Western blot. We found that PTPN2 (45 kDa and 48 kDa) over-expression inhibits protein expression of GRP78, P-IRE1, IRE1, XBP1, P-PERK, PERK, and P-EIF2 $\alpha$ , but does NOT alter ATF-6 expression in TG-treated TNBC cells. These results not only indicate that PTPN2 (45 kDa and 48 kDa) over-expression inhibits both the IRE1-XBP1 and PERK/EIF2 $\alpha$ /ATF4 pathways, but also has no significant effect on the ATF-6 pathway in TG-treated MDA-MB-231 and SUM159 cells (Fig. 2C).

In addition, we found that PTPN2 knockdown enhances mRNA expression of GRP78, IRE1, XBP1, ATF-4, and ATF-6 in TG-treated, but not in DMSO-treated MDA-MB-231 and SUM159 cells in general (Fig. 2D,E). Furthermore, PTPN2 knockdown enhances protein expression of GRP78, P-IRE1, IRE1, XBP1, P-PERK, PERK, and P-EIF2 $\alpha$ , but does NOT alter ATF-6 expression in TG-treated TNBC cells. These results not only indicate that PTPN2 knockdown stimulates both the IRE1-XBP1 and PERK/EIF2 $\alpha$ /ATF4 pathways but also has no significant effect on the ATF-6 pathway in TG-treated MDA-MB-231 and SUM159 cells (Fig. 2F).

In this study, we used another ERS-inducing agent, tunicamycin (TM) to treat PTPN2 knockdown MDA-MB-231 and SUM159 cells. Our results demonstrated that PTPN2 knockdown decreases mRNA expression of GRP78, XBP1, and ATF-6 in TM-treated MDA-MB-231 cells but PTPN2 knockdown increases mRNA expression of GRP78 and ATF6 in TM-treated SUM159 cells (Supplementary Fig. 2A and 2B). Moreover, PTPN2 knockdown shows no significant effect on protein expression of ERS markers (i.e., GRP78, P-IRE1, IRE1, P-PERK, PERK, P-EIF2 $\alpha$ , and ATF-6) in TM-treated MDA-MB-231 and SUM159 cells (Supplementary Fig. 2C). Thus, we focused our study on the role of PTPN2 in TG-induced ERS.

### PTPN2 promotes cell proliferation and inhibits cell apoptosis in TG-treated TNBC cells

In general, cells possess the ability to restore proteostasis and survive under temporary and mild ERS conditions, but cells will undergo cell death by utilizing multiple signaling pathways (including apoptosis) under sustained and severe ERS conditions. In order to demonstrate the effect of PTPN2 on TG-treated TNBC cells, we examined cell proliferation and cell apoptosis. The EdU staining results showed that PTPN2 (45 kDa and 48 kDa) over-expression significantly increases cell proliferation in TG-treated MDA-MB-231 cells (Fig. 3A,B). Whereas, PTPN2 (45 kDa and 48 kDa) over-expression significantly increases cell proliferation in DMSO-treated MDA-MB-231 cells (Fig. 3A,B). These results indicate that PTPN2 plays a cell proliferation role in TG-treated versus DMSO-treated MDA-MB-231 cells. Moreover, we found that PTPN2 (45 kDa and 48 kDa) over-expression reduces the number of apoptotic cells in TG-treated MDA-MB-231 and SUM159 cells by flow cytometry using Annexin V/ Propidium Iodide (PI) staining (Fig. 3C–E). Western blot results confirmed that PTPN2 (45 kDa and 48 kDa) over-expression increases cell proliferation by enhancing PCNA expression and decreases cell apoptosis by diminishing cleaved caspase3 and cleaved PARP expression in TG-treated MDA-MB-231 cells (Fig. 3F).

Furthermore, PTPN2 knockdown decreases cell proliferation illustrated by EdU staining (Supplementary Fig. 3A & B) and cell viability by live/dead cell staining (Supplementary Fig. 3C & D) in TG-treated MDA-MB-231 cells. Moreover, PTPN2 knockdown increases the number of apoptotic cells in TG-treated MDA-MB-231 and SUM159 cells (Supplementary Fig. 3E & F) by flow cytometry using Annexin V/ PI staining. PTPN2 knockdown also increases the number of apoptotic cells shown by Hoechst 33,342 staining with intense staining in the nucleus in TG-treated MDA-MB-231 cells (Supplementary Fig. 3G & H).

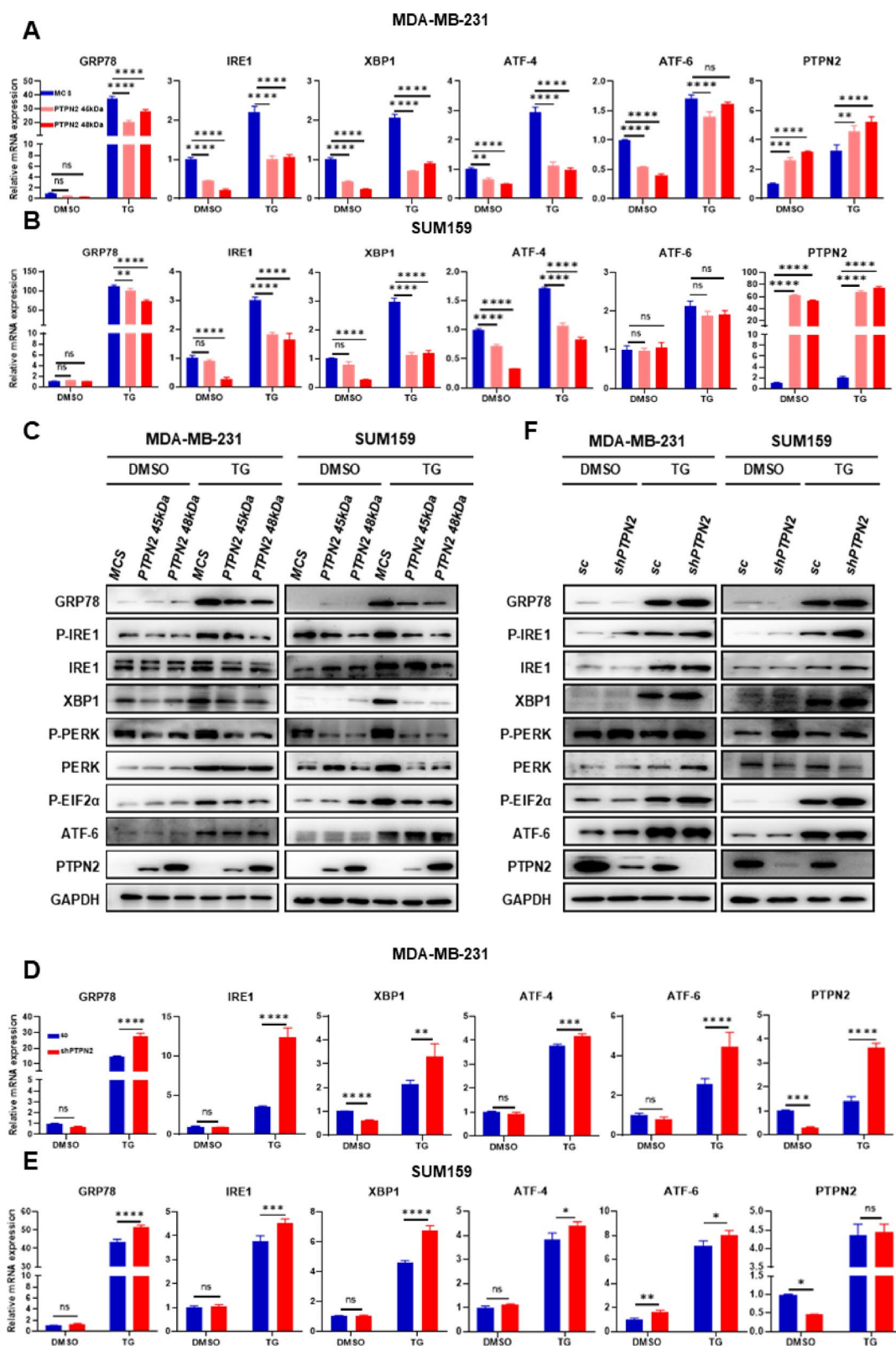
In addition, the ex vivo results confirmed that PTPN2 knockout decreases cell proliferation (i.e., Ki67, Fig. 3G,H) and increases cell apoptosis (i.e., cleaved Caspase3, Fig. 3I,J) in TG-treated 4T1 murine breast carcinoma tissues by immunohistochemistry staining.

### PTPN2 inhibits TG-induced TNBC cell apoptosis through the mitochondrial pathway

The above-mentioned results indicate that PTPN2 is only involved in TG-induced ERS, but not TM-induced ERS. TG interrupts Ca<sup>2+</sup> homeostasis in the ER, and ER-mitochondria tethering is important for Ca<sup>2+</sup> buffering and apoptosis. Thus, we next examined mitochondrial Ca<sup>2+</sup> levels. We found that PTPN2 (45 kDa and 48 kDa) over-expression decreases mitochondrial Ca<sup>2+</sup> levels, whereas PTPN2 knockdown increases mitochondrial Ca<sup>2+</sup> levels in TG-treated MDA-MB-231 cells using Mito-Tracker and Rhod-2 immunofluorescence staining (Fig. 4A,B).

The dysregulation of mitochondrial Ca<sup>2+</sup> homeostasis plays a critical role in ROS production which associates with regulation of apoptosis. Thus, we then examined ROS levels using immunofluorescence. Our results showed that PTPN2 (45 kDa and 48 kDa) over-expression decreases ROS production, whereas PTPN2 knockdown increases ROS production in TG-treated MDA-MB-231 cells (Fig. 4C–F). We further examined the expression of CHOP (an apoptosis inducer in ERS pathway), AMPK (a major energy sensor), Bax and Bcl-2 (mitochondrial apoptosis-related proteins) which are involved in TG-induced apoptosis using Western blots. Our results demonstrated that PTPN2 (45 kDa and 48 kDa) over-expression not only decreases the expression of CHOP, P-AMPK, and Bax, but also increases the expression of Bcl-2 which decreases the Bax/Bcl-2 ratio in TG-treated MDA-MB-231 cells (Fig. 4G). The Western blot results of PTPN2 knockdown showed opposite findings (Fig. 4H).

In addition, the ex vivo results confirmed that PTPN2 knockout increases CHOP expression in TG-treated 4T1 murine breast carcinoma tissues by immunohistochemistry staining (Fig. 4I,J). The Western blot results also showed that PTPN2 knockout increases GRP78 and CHOP expression in TG-treated 4T1 murine breast carcinoma tissues (Fig. 4K).



### PTPN2 inhibits TG-induced TNBC autophagy functioning as a defender for cell apoptosis

Since ERS also activates autophagy that degrades misfolded/unfolded proteins when ERAD cannot address it, we next examined the role of PTPN2 in TG-induced autophagy.

We found that PTPN2 (45 kDa and 48 kDa) over-expression diminishes the up-regulation of the LC3 II/LC3 I ratio (an autophagy marker protein) and enhances p62 expression in TG-treated MDA-MB-231 and SUM159 cells using Western blot analysis (Fig. 5A). The Western blot results of PTPN2 knockdown showed the opposite findings (Fig. 5B).

◀ **Fig. 2.** PTPN2 inhibits TG-initiated ERS through IRE1-XBP1 and PERK/EIF2 $\alpha$ /ATF-4 pathways in TNBC. (A & B) The bar graph shows that ectopic expression of PTPN2 45 kDa or PTPN2 48 kDa inhibits expression of key molecules in IRE1 and PERK pathways in TG-treated MDA-MB-231 (A) and SUM159 (B) cells by qPCR. All experiments were conducted three times independently (n = 3). (C) The Western blot shows that ectopic expression of PTPN2 45 kDa or PTPN2 48 kDa inhibits expression of key molecules in IRE1 and PERK pathways in TG-treated MDA-MB-231 and SUM159 cells. PTPN2 serves to indicate over-expression of PTPN2, and GAPDH serves as a loading control. All experiments were conducted two times independently (n = 2). (D & E) The bar graph shows that knockdown of PTPN2 augments expression of key molecules in IRE1 and PERK pathways in TG-treated MDA-MB-231 (D) and SUM159 (E) cells by qPCR. All experiments were conducted three times independently (n = 3). (F) The Western blot shows that knockdown of PTPN2 augments expression of key molecules in IRE1 and PERK pathways in TG-treated MDA-MB-231 and SUM159 cells. PTPN2 serves to indicate knockdown of PTPN2, and GAPDH serves as a loading control. All experiments were conducted two times independently (n = 2).

Since PTPN2 inhibits both TG-induced cell apoptosis and autophagy, we then investigated the contribution of autophagy to apoptosis under TG-induced condition with modified PTPN2 expression. We treated MDA-MB-231 cells using TG with or without chloroquine (CQ; an autophagy inhibitor) followed by Annexin V/ PI staining. Our results showed that PTPN2 knockdown significantly increases the percentage of apoptotic cells in TG-treated MDA-MB-231 cells. Co-treatment with TG and CQ further increases the percentage of apoptotic cells compared to TG-treated MDA-MB-231 cells under PTPN2 knockdown conditions (Fig. 5C,D). Moreover, we found that PTPN2 knockdown increases the expression of Cleaved caspase3 and the ratio of LC3 II/LC3 I in TG-treated MDA-MB-231 cells using Western blot analysis. Co-treatment with TG and CQ further increases the expression of Cleaved caspase3 and the ratio of LC3 II/LC3 I compared to TG-treated MDA-MB-231 cells under PTPN2 knockdown conditions (Fig. 5D,E). The above results collectively indicate that TG-induced autophagy protects cells from apoptosis under PTPN2 knockdown conditions.

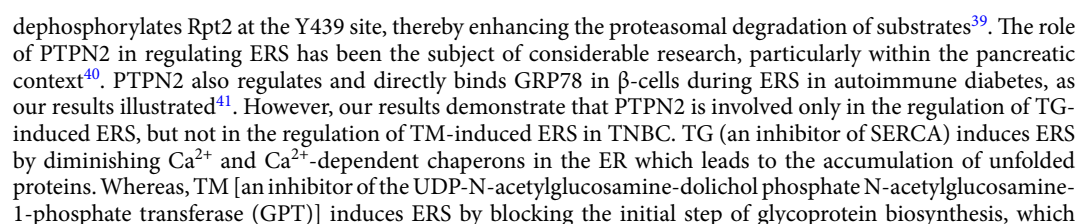
## Discussion

The prognosis for TNBC patients is poor and recurrence is common due to limited treatment options<sup>5,27</sup>. Although application of ICIs has improved PFS and OS of certain TNBC patients, the majority do not exhibit significant benefits, and there are inherent limitations associated with ICI therapy. Therefore, the need to explore other avenues in TNBC treatment remains a fertile ground for exploration. In this study, we propose that PTPN2 suppresses TG-induced ERS and the subsequent apoptosis via the following routes: (1) PTPN2 inhibits activation of the IRE1-XBP1 and PERK/ EIF2 $\alpha$ /ATF-4 signaling pathways by preventing the phosphorylation of IRE1, PERK and EIF2 $\alpha$ , phosphorylation of IRE1, PERK and EIF2 $\alpha$ , (2) TG-induced ERS and the subsequent apoptosis occurs via the regulation of Ca<sup>2+</sup> homeostasis and ROS production, (3) PTPN2 inhibits TG-induced apoptosis via the mitochondrial apoptosis pathway (CHOP, AMPK, and Bax/Bcl-2 ratio are pivotal factors), and (4) the concurrent activation of autophagy serves as a protective mechanism against TG-induced apoptosis (Fig. 6).

PTPN2 has garnered significant interest due to its pivotal role as a potential target for cancer immunotherapy<sup>21,22</sup>. Tumors are categorized into immune-cold tumors, such as breast cancer, ovarian cancer, and prostate cancer, and immune-hot tumors, including melanoma and non-small cell lung cancer, based on T cell infiltration and the levels of pro-inflammatory cytokines<sup>28–30</sup>. PTPN2 is regarded as a highly promising target for immunotherapy, particularly in enhancing interferon-gamma (IFN- $\gamma$ ) signaling networks and the subsequent response to immune checkpoint inhibitor (ICI) therapy in both immune-cold and immune-hot tumors. The functionality of PTPN2 is primarily mediated through the JAK/STAT signaling pathway<sup>31</sup>, although interactions with other pathways, including protein kinase B (AKT), Src family kinase (SFK), and MEK/ERK, have also been documented<sup>32–34</sup>. The deletion of PTPN2 in tumor cells has been shown to enhance the efficacy of immunotherapy by increasing STAT1 phosphorylation mediated by interferon- $\gamma$ , as well as the expression of molecules related to antigen processing and presentation (such as B2m, MHC-I, and MHC-II) and certain chemokines (including Cxcl9, Cxcl10, and Cxcl11). This upregulation facilitates T cell infiltration into the tumor, ultimately leading to tumor growth suppression<sup>21</sup>. Furthermore, elevated levels of PTPN2 have been observed in human cancers that exhibit resistance to existing immunotherapeutic strategies<sup>35</sup>. An increasing number of comprehensive studies have implicated PTPN2 in cancer-promoting effects and adverse prognoses<sup>35,36</sup>. Currently, there is no commercially available small inhibitor specifically targeting PTPN2, primarily due to the structural similarities between PTPN1 and PTPN2. Nevertheless, small inhibitors that target both PTPN1 and PTPN2, either ABBV-CLS-484 or Compound-182, has demonstrated the potential to enhance T cell-mediated anti-tumor immunity<sup>24,25</sup>. However, the lack of specificity for each target complicates the assessment of the clinical benefits associated with immunotherapy directed at these molecules. In the 2024 ASCO Annual Meeting, Li et al. presented HDM2010, a highly potent inhibitor of PTPN2<sup>26</sup>. While this compound exhibits a favorable pharmacokinetic and safety profile, further optimization through preclinical models is still ongoing.

In our study, we have shown that PTPN2 inhibits ubiquitin-dependent protein degradation, which disrupts proteostasis and influences occurrence of ERS. Moreover, PTPN2 regulates and directly interacts with GRP78 (the master regulator of UPR) which indicates that PTPN2 associates with ERS. The human 26S proteasome has been shown to contain 453 phosphorylation sites using protein profiling analysis, 143 (nearly 33%) of which are tyrosine phosphorylation sites<sup>37,38</sup>. For example, a variety of receptor tyrosine kinases (RTKs) promote phosphorylation at Y439 site of Rpt2 subunit in 19S regulatory particle through the activation of Src, which disrupts the functionality of the 26S proteasome. Additionally, PTPN2, with a molecular weight of 48 kDa,







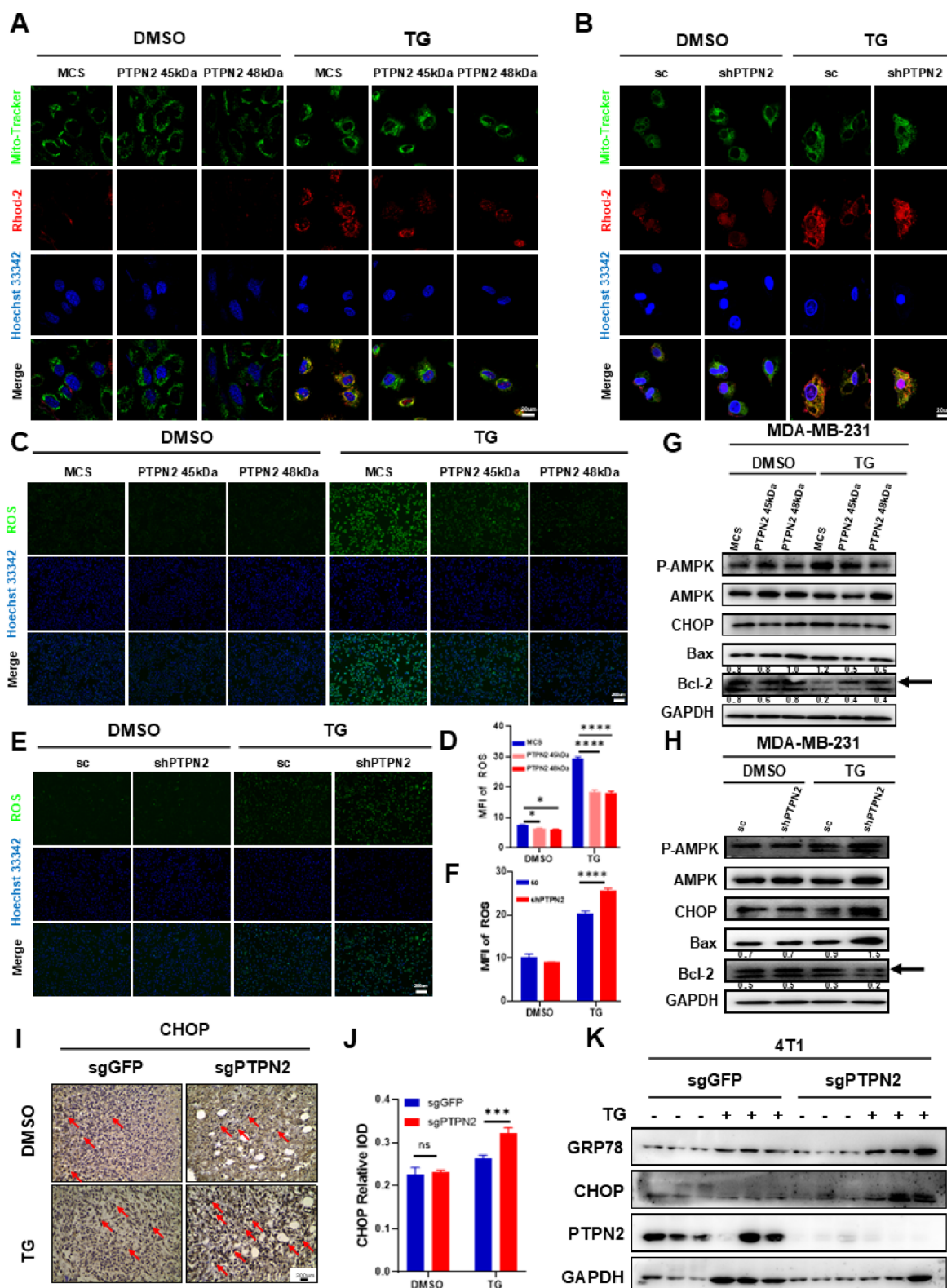
◀ **Fig. 3.** PTPN2 promotes TG-initiated cell proliferation and inhibits TG-initiated apoptosis in TNBC cells. **(A)** The representative fluorescence images of EdU staining shows that ectopic expression of PTPN2 45 kDa or PTPN2 48 kDa promotes cell proliferation in TG-treated MDA-MB-231 cells. Scale bar = 100  $\mu$ m. All experiments were conducted three times independently ( $n = 3$ ). **(B)** The bar graph shows that ectopic expression of PTPN2 45 kDa or PTPN2 48 kDa promotes cell proliferation in TG-treated MDA-MB-231 cells by quantifying EdU positive cells in 3 different fields under the microscope. **(C)** The representative flow cytometry images of MDA-MB-231 and SUM159 cells staining with Annexin V/PI indicating percentage of apoptosis. All experiments were conducted three times independently ( $n = 3$ ). **(D & E)** The bar graph shows ectopic expression of PTPN2 45 kDa or PTPN2 48 kDa inhibits percentage of apoptotic cells in TG-treated MDA-MB-231 **(D)** and SUM159 **(E)** cells based on flow cytometry detection of Annexin V/PI staining cells. **(F)** The Western blot shows that ectopic expression of PTPN2 45 kDa or PTPN2 48 kDa promotes cell proliferation (PCNA) and inhibits apoptosis (cleaved Caspase3 & cleaved PARP) in TG-treated MDA-MB-231 cells. GAPDH serves as a loading control. All experiments are conducted as a single independent experiment ( $n = 1$ ). **(G)** The representative Ki67 immunohistochemical staining images of TG-treated 4T1 tissues in ex vivo. Scale bar = 200  $\mu$ m. Each experimental group has three samples ( $n = 3$ ). **(H)** The bar graph demonstrates that knockout of PTPN2 significantly inhibits proliferation of TG-treated 4T1 tissues in ex vivo. **(I)** The representative cleavage Caspase3 immunohistochemical staining images of TG-treated 4T1 tissues in ex vivo. Scale bar = 200  $\mu$ m. Each experimental group has three samples ( $n = 3$ ). **(J)** The bar graph demonstrates that knockout of PTPN2 significantly promotes apoptosis of TG-treated 4T1 tissues in ex vivo.

leads to the accumulation of unfolded glycoproteins<sup>42</sup>. Elvira et al. reported that PTPN2 associates with the regulation of TG-induced ERS but not with the regulation of TM-induced ERS in pancreatic  $\beta$  cells. Moreover, TM treatment does not alter the expression of ERS-related proteins<sup>41</sup>. However, we cannot rule out the possibility that the involvement of PTPN2 in TM-treated TNBC may occur through other mechanisms. In this regard, PD-L1 located on the cell membrane of cancer cells is highly glycosylated which ensures its stability and affinity with PD-1<sup>43</sup>. Consequently, we speculate that targeting PD-L1 glycosylation by TM may influence the immune response and ICI efficacy in TNBC.

IRE1 is the most evolutionary conserved signal in response to the accumulation of misfolded proteins. The IRE1a RNase regulatory network is dynamically fine-tuned by tyrosine kinases and phosphatases when placed under various stresses. The phosphorylation of RtcB (a tRNA ligase responsible for XBP1 mRNA splicing) at Y306 perturbs RtcB interaction with IRE1 $\alpha$ , thereby attenuating XBP1 mRNA splicing<sup>44</sup>. Our results show that PTPN2 attenuates TG-induced IRE1 phosphorylation and XBP1 expression in TNBC cells. This study shows for the first time that PTPN2 mediates IRE1 phosphorylation and influences IRE1-XBP1 pathway, although the exact mechanism remains unclear. In addition, this study also shows that PTPN2 attenuates TG-induced ERS through PERK/EIF2 $\alpha$ /ATF-4 pathways in TNBC cells. Elvira et al. revealed that PTPN2 participates in ERS via regulation of the PERK/EIF2 $\alpha$ /ATF-4 signaling pathway in pancreatic  $\beta$  cells<sup>41</sup>. PTPN2 knockdown enhances mRNA and protein expression of EIF2 $\alpha$  and ATF-4 in TG-treated EndoC- $\beta$ H1 cells and prompts activation of the PERK/EIF2 $\alpha$ /ATF4 pathway<sup>41</sup>.

The findings of our study indicate that treatment with TG results in a reduction of cell proliferation and an increase in apoptosis among TNBC cells. Conversely, PTPN2 appears to counteract the effects of TG by alleviating the reduction in cell proliferation and the enhancement of apoptosis induced by TG. Furthermore, TG treatment also destroys the  $\text{Ca}^{2+}$  homeostasis between the ER and the cytosol/mitochondria which indicates that the  $\text{Ca}^{2+}$  signaling pathway plays an important role in ERS-induced apoptosis. Imbalance of  $\text{Ca}^{2+}$  causes a series of biochemical changes which include: (1) ROS production, (2) mitochondrial permeability transition pore opening, (3) Cyto c, AIF, and Bax (pro-apoptotic proteins) release from the ER, (4) Bax/Bcl-2 ratio up-regulation, (5) caspase activation, and (6) mitochondrial apoptosis pathway activation<sup>45,46</sup>. We observed PTPN2 decreases mitochondrial  $\text{Ca}^{2+}$  levels and ROS production in TG-treated TNBC cells with diminished CHOP expression, AMPK stimulation, and Bax/Bcl-2 ratio which may occur due to the activation of IRE1-XBP1 and PERK/EIF2 $\alpha$ /ATF-4 pathways. However, expression of other molecules associated with  $\text{Ca}^{2+}$  transport, for example IP3Rs (a  $\text{Ca}^{2+}$  release channel mainly located in the ER), GRP75 (a mitochondrial chaperone protein) and VDAC (a voltage-dependent anion channel) need to be explored<sup>47</sup>. A previous study showed that the IRE1-XBP1 signaling pathway participates in TG-induced apoptosis in a cell-specific manner, which was pro-apoptotic in human prostate cancer LNCaP cells, but not in human colon cancer HCT116 cells<sup>48</sup>. This difference in TG-induced apoptosis between LNCaP cells and HCT116 cells depends on the XBP1-dependent activation of c-Jun N-terminal kinase<sup>49</sup>. PERK (a regulator of ERS) contributes to apoptosis by phosphorylation of EIF2 $\alpha$  and by translation of ATF-4 thereby initiating transcription of CHOP which regulates ERS-induced apoptosis<sup>50,51</sup>. Moreover, PERK promotes protective mitochondrial elongation by adaptive remodeling of mitochondrial membrane phosphatidic acid and by interacting with ATAD3A (a mitochondrial protein) during ER stress, which forms mitochondria-ER contact sites<sup>52,53</sup>. Whether PTPN2 plays a role in the above-mentioned processes needs further investigation.

mTOR is commonly considered a negative regulator of autophagy whereby AMPK activation inhibits mTOR activity and thereby initiates autophagy. Autophagy mediated by the PERK/AMPK/mTORC1 pathway occurs in endothelial cells during ECM detachment<sup>54</sup>. Our results showed that TG treatment activates AMPK phosphorylation and that PTPN2 decreases TG-induced AMPK phosphorylation. Aradi et al. reported that PTPN2 silencing increases both autophagy and the formation of autophagosomes in TG-treated synovial fibroblasts<sup>55</sup>. A previous report showed that PERK signaling decides the fate of a cell during ERS due to its autophagy-apoptosis switching role and that P38 links the crosstalk between autophagy and apoptosis initiated



by PERK<sup>56</sup>. Under intermittent or mild ERS, autophagy promotes cell survival by activating the autophagy-lysosomal degradation pathway to degrade misfolded proteins. However, sustained and severe ERS conditions lead to excessive autophagy and eventually to apoptosis<sup>27</sup>. Under our experimental conditions, we found that autophagy protects against apoptosis. However, other investigators showed that both Caspase protein expression and the proportion of apoptotic cells increase in the presence of autophagy inhibitors in TG- or TM-treated HepG2 cells<sup>57,58</sup>. Moreover, the cell apoptosis induced by TG and TM can be partially rescued by autophagy which indicates that autophagy protects cells from apoptosis and promotes cell survival<sup>57,58</sup>.

PTPN2 deletion in cancer cells increases immunotherapy efficacy by enhancing interferon- $\gamma$ -mediated effects on antigen presentation and growth suppression, which suggests that PTPN2 may serve as an efficacious

◀ **Fig. 4.** PTPN2 inhibits TG-initiated apoptosis through the  $\text{Ca}^{2+}$ / ROS/ mitochondrial pathway. (A) The representative fluorescence images of Mito Tracker (green)/ Rhod-2 (red) staining demonstrating  $\text{Ca}^{2+}$  level in the mitochondria shows that ectopic expression of PTPN2 45 kDa or PTPN2 48 kDa decreases  $\text{Ca}^{2+}$  level in the mitochondria in TG-treated MDA-MB-231 cells. Hoechst 33,342 staining indicates nuclei. Scale bar = 20  $\mu\text{m}$ . All experiments are conducted as a single independent experiment ( $n = 1$ ). (B) The representative fluorescence images of Mito Tracker (green)/ Rhod-2 (red) staining demonstrating  $\text{Ca}^{2+}$  level in the mitochondria shows that knockdown of PTPN2 increases  $\text{Ca}^{2+}$  level in the mitochondria in TG-treated MDA-MB-231 cells. Hoechst 33,342 staining indicates nuclei. Scale bar = 20  $\mu\text{m}$ . All experiments are conducted as a single independent experiment ( $n = 1$ ). (C) The representative fluorescence images of DCFH-DA staining demonstrating ROS level shows that ectopic expression of PTPN2 45 kDa or PTPN2 48 kDa decreases ROS production in TG-treated MDA-MB-231 cells. Hoechst 33,342 staining indicates nuclei. Scale bar = 200  $\mu\text{m}$ . All experiments were conducted three times independently ( $n = 3$ ). (D) The bar graph shows that ectopic expression of PTPN2 45 kDa or PTPN2 48 kDa inhibits ROS production in TG-treated MDA-MB-231 cells by measuring mean fluorescence intensity of green fluorescent cells in 3 different fields under the microscope. (E) The representative fluorescence images of DCFH-DA staining demonstrating ROS level shows that knockdown of PTPN2 increases ROS production in TG-treated MDA-MB-231 cells. Hoechst 33,342 staining indicates nuclei. Scale bar = 200  $\mu\text{m}$ . All experiments were conducted three times independently ( $n = 3$ ). (F) The bar graph shows that knockdown of PTPN2 promotes ROS production in TG-treated MDA-MB-231 cells by measuring mean fluorescence intensity of green fluorescent cells in 3 different fields under the microscope. (G) The western blot shows that ectopic expression of PTPN2 45 kDa or PTPN2 48 kDa decreases expression of CHOP, P-AMPK and Bax, and increases expression of Bcl-2 in TG-treated MDA-MB-231 cells. GAPDH serves as a loading control. All experiments are conducted as a single independent experiment ( $n = 1$ ). (H) The western blot shows that knockdown of PTPN2 increases expression of CHOP, P-AMPK and Bax, and decreases expression of Bcl-2 in TG-treated MDA-MB-231 cells. GAPDH serves as a loading control. All experiments are conducted as a single independent experiment ( $n = 1$ ). (I) The representative CHOP immunohistochemical staining images of TG-treated 4T1 tissues in ex vivo. Scale bar = 200  $\mu\text{m}$ . Each experimental group has three samples ( $n = 3$ ). (J) The bar graph demonstrates that knockout of PTPN2 significantly promotes CHOP expression of TG-treated 4T1 tissues in ex vivo. (K) The western blot shows that PTPN2 knockout promotes GRP78 and CHOP expression of TG-treated 4T1 tissues in ex vivo. GAPDH serves as a loading control.

immunotherapy target<sup>21</sup>. The collective findings from our study demonstrate that the presence of TG reverses the impact of PTPN2 on cancer cell proliferation. Specifically, the knockdown of PTPN2 leads to an increase in cancer cell proliferation in the absence of TG, while it results in a decrease in proliferation when TG is present. Therefore, we propose that a combined therapeutic approach utilizing a PTPN2 inhibitor alongside TG may effectively inhibit cancer cell growth, potentially through mechanisms involving interferon- $\gamma$ -mediated T cell anti-tumor responses or by promoting enhanced apoptosis of the cancer cells themselves.

## Conclusion

The treatment of TNBC patients is limited, and it is necessary to explore new TNBC treatment methods. This study posits that PTPN2 plays a role in the suppression of TG-induced ERS and the ensuing apoptotic processes. Therefore, inhibiting the expression of PTPN2 in TNBC, alongside the induction of ERS, may represent a promising new approach for the treatment of this malignancy, potentially expanding the therapeutic landscape for TNBC management.

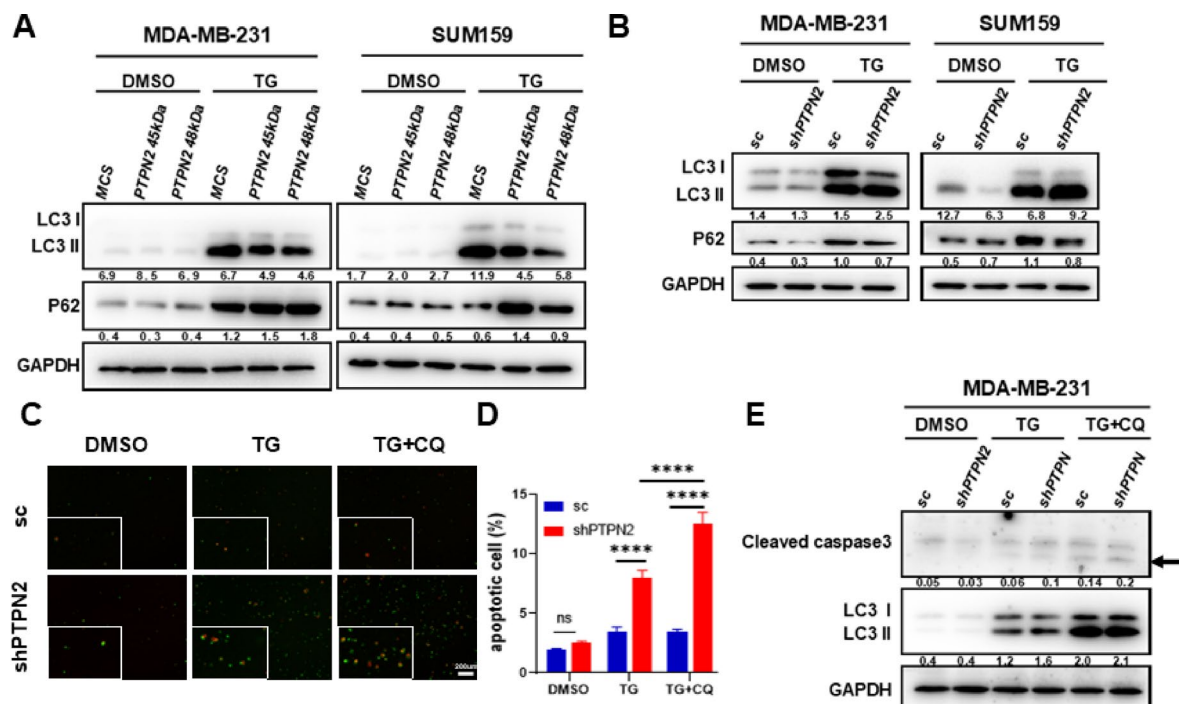


**Fig. 5.** PTPN2 inhibits TG-initiated autophagy in TNBC. (A) The western blot shows that ectopic expression of PTPN2 45 kDa or PTPN2 48 kDa decreases LC3 II/LC3 I ratio and increases P62 expression, indicating PTPN2 inhibits autophagy in TG-treated MDA-MB-231 and SUM159 cells. GAPDH serves as a loading control. All experiments were conducted two times independently (n = 2). (B) The western blot shows that knockdown of PTPN2 increases LC3 II/LC3 I ratio and decreases P62 expression, indicating knockdown of PTPN2 promotes autophagy in TG-treated MDA-MB-231 and SUM159 cells. GAPDH serves as a loading control. All experiments were conducted two times independently (n = 2). (C) The representative fluorescence images of Annexin V/ PI staining demonstrating apoptotic cells shows that knockdown of PTPN2 promotes cell apoptosis in TG-treated MDA-MB-231 cells, and the presence of CQ further elevates cell apoptosis. Scale bar = 200um. All experiments were conducted three times independently (n = 3). (D) The bar graph shows that knockdown of PTPN2 promotes cell apoptosis in TG-treated MDA-MB-231 cells, and the presence of CQ further elevates cell apoptosis by quantifying apoptotic cells in 3 different fields under the microscope. (E) The western blot shows that knockdown of PTPN2 increases expression of cleaved Caspase3 and the ratio of LC3 II/LC3 I. Presence of CQ further elevates expression of cleaved Caspase3 and the ratio of LC3 II/LC3 I, indicating CQ presence promotes apoptosis in TG-treated MDA-MB-231 cells. GAPDH serves as a loading control. All experiments are conducted as a single independent experiment (n = 1).



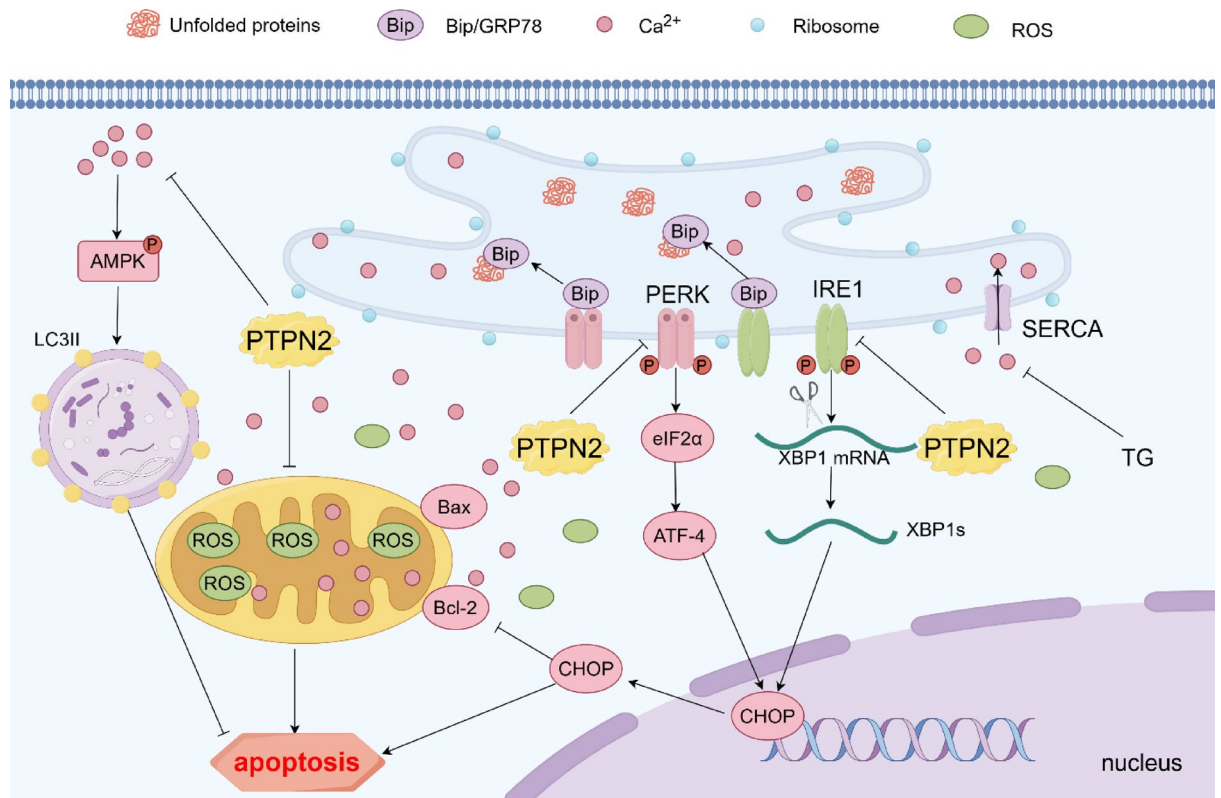


**Fig. 6.** A schematic diagram of the regulatory mechanism by which PTPN2 inhibits TG-induced endoplasmic reticulum stress and subsequent cell apoptosis. PTPN2 inhibits the activation of the IRE1-XBP1 and PERK/EIF2 $\alpha$ /ATF-4 signaling pathways by preventing the phosphorylation of IRE1, PERK, and EIF2 $\alpha$ , and TG-induced ER stress and subsequent cell apoptosis through the regulation of Ca<sup>2+</sup> homeostasis and ROS production. PTPN2 inhibits TG-induced cell apoptosis through the mitochondrial apoptosis pathway (with CHOP, AMPK, and the Bax/Bcl-2 ratio being key factors); PTPN2 activates protective mechanisms against TG-induced apoptosis during the process of autophagy.

## Data availability

Data is provided within the manuscript or supplementary information files.

Received: 9 December 2024; Accepted: 26 May 2025

Published online: 06 June 2025

## References

1. Siegel, R. L., Miller, K. D., Wagle, N. S. & Jemal, A. Cancer statistics, 2023. *CA Cancer J. Clin.* **73**(1), 17–48 (2023).
2. Garrido-Castro, A. C., Lin, N. U. & Polyak, K. Insights into molecular classifications of triple-negative breast cancer: Improving patient selection for treatment. *Cancer Discov.* **9**(2), 176–198 (2019).
3. Goldhirsch, A. et al. Personalizing the treatment of women with early breast cancer: Highlights of the St Gallen international expert consensus on the primary therapy of early breast cancer 2013. *Ann. Oncol.* **24**(9), 2206–2223 (2013).
4. Foulkes, W. D., Smith, I. E. & Reis-Filho, J. S. Triple-negative breast cancer. *N. Engl. J. Med.* **363**(20), 1938–1948 (2010).
5. Caswell-Jin, J. L. et al. Change in survival in metastatic breast cancer with treatment advances: Meta-analysis and systematic review. *JNCI Cancer Spectr.* **2**(4), 062 (2018).
6. O'Shaughnessy, J. et al. Phase III study of iniparib plus gemcitabine and carboplatin versus gemcitabine and carboplatin in patients with metastatic triple-negative breast cancer. *J. Clin. Oncol.* **32**(34), 3840–3847 (2014).
7. Jia, H. et al. Immunotherapy for triple-negative breast cancer: Existing challenges and exciting prospects. *Drug Resist. Update* **32**, 1–15 (2017).
8. Hetz, C., Chevet, E. & Oakes, S. A. Proteostasis control by the unfolded protein response. *Nat. Cell Biol.* **17**(7), 829–838 (2015).
9. Voeltz, G. K., Rolls, M. M. & Rapoport, T. A. Structural organization of the endoplasmic reticulum. *EMBO Rep.* **3**(10), 944–950 (2002).
10. Guan, B.-J. et al. Translational control during endoplasmic reticulum stress beyond phosphorylation of the translation initiation factor eIF2 $\alpha$ . *J. Biol. Chem.* **289**(18), 12593–12611 (2014).
11. Markouli, M., Strepkos, D., Papavassiliou, A. G. & Piperi, C. Targeting of endoplasmic reticulum (ER) stress in gliomas. *Pharmacol. Res.* **157**, 104823 (2020).
12. Amen, O. M., Sarker, S. D., Ghildyal, R. & Arya, A. Endoplasmic reticulum stress activates unfolded protein response signaling and mediates inflammation, obesity, and cardiac dysfunction: Therapeutic and molecular approach. *Front. Pharmacol.* **10**, 977 (2019).
13. Hetz, C., Zhang, K. & Kaufman, R. J. Mechanisms, regulation and functions of the unfolded protein response. *Nat. Rev. Mol. Cell Biol.* **21**(8), 421–438 (2020).
14. Hetz, C. & Papa, F. R. The unfolded protein response and cell fate control. *Mol. Cell* **69**(2), 169–181 (2018).

15. Walter, P. & Ron, D. The unfolded protein response: From stress pathway to homeostatic regulation. *Science* **334**(6059), 1081–1086 (2011).
16. Tiganis, T. & Bennett, A. M. Protein tyrosine phosphatase function: The substrate perspective. *Biochem. J.* **402**(1), 1–15 (2007).
17. van Vliet, C. et al. Selective regulation of tumor necrosis factor-induced Erk signaling by Src family kinases and the T cell protein tyrosine phosphatase. *Nat. Immunol.* **6**(3), 253–260 (2005).
18. Klingler-Hoffmann, M. et al. The protein tyrosine phosphatase TCPTP suppresses the tumorigenicity of glioblastoma cells expressing a mutant epidermal growth factor receptor. *J. Biol. Chem.* **276**(49), 46313–46318 (2001).
19. Mattila, E., Auvinen, K., Salmi, M. & Ivaska, J. The protein tyrosine phosphatase TCPTP controls VEGFR2 signalling. *J. Cell Sci.* **121**(Pt 21), 3570–3580 (2008).
20. Simoncic, P. D., Lee-Loy, A., Barber, D. L., Tremblay, M. L. & McGlade, C. J. The T cell protein tyrosine phosphatase is a negative regulator of Janus family kinases 1 and 3. *Curr. Biol.* **12**(6), 446–453 (2002).
21. Manguso, R. T. et al. In vivo CRISPR screening identifies Ptpn2 as a cancer immunotherapy target. *Nature* **547**(7664), 413–418 (2017).
22. Song, J., Lan, J., Tang, J. & Luo, N. PTPN2 in the Immunity and Tumor Immunotherapy: A Concise Review. *Int J Mol Sci* **23**(17), 10025 (2022).
23. Stanford, S. M. & Bottini, N. Targeting protein phosphatases in cancer immunotherapy and autoimmune disorders. *Nat. Rev. Drug Discovery* **22**(4), 273–294 (2023).
24. Baumgartner, C. K. et al. The PTPN2/PTPN1 inhibitor ABBV-CLS-484 unleashes potent anti-tumour immunity. *Nature* **622**(7984), 850–862 (2023).
25. Liang, S. et al. A small molecule inhibitor of PTP1B and PTPN2 enhances T cell anti-tumor immunity. *Nat. Commun.* **14**(1), 4524 (2023).
26. Li, K., Min, C., Zhang, Z. & Liu, D. Discovery of HDM2010, a highly potent PTPN2 inhibitor for immunotherapy. *J. Clin. Oncol.* **42**(16\_suppl), e15021–e15021 (2024).
27. Qi, Z. & Chen, L. Endoplasmic reticulum stress and autophagy. *Adv. Exp. Med. Biol.* **1206**, 167–177 (2019).
28. Duan, Q., Zhang, H., Zheng, J. & Zhang, L. Turning cold into hot: Firing up the tumor microenvironment. *Trends Cancer* **6**(7), 605–618 (2020).
29. Galon, J. & Bruni, D. Approaches to treat immune hot, altered and cold tumours with combination immunotherapies. *Nat. Rev. Drug Discov.* **18**(3), 197–218 (2019).
30. Xiao, Y. et al. Multi-omics profiling reveals distinct microenvironment characterization and suggests immune escape mechanisms of triple-negative breast cancer. *Clin. Cancer Res.: Off. J. Am. Assoc. Cancer Res.* **25**(16), 5002–5014 (2019).
31. Luo, N. et al. Melanoma response to anti-PD-L1 immunotherapy requires JAK1 signaling, but not JAK2. *Oncoimmunology* **7**(6), e1438106 (2018).
32. Feng, Y. et al. Genetic variants of PTPN2 are associated with lung cancer risk: A re-analysis of eight GWASs in the TRICL-ILCCO consortium. *Sci. Rep.* **7**(1), 825 (2017).
33. Goh, P. K. et al. PTPN2 elicits cell autonomous and non-cell autonomous effects on antitumor immunity in triple-negative breast cancer. *Sci. Adv.* **8**(8), eabk3338 (2022).
34. Tang, X., Qi, C., Zhou, H. & Liu, Y. Critical roles of PTPN family members regulated by non-coding RNAs in tumorigenesis and immunotherapy. *Front. Oncol.* **12**, 972906 (2022).
35. Tang, X., Sui, X. & Liu, Y. Immune checkpoint PTPN2 predicts prognosis and immunotherapy response in human cancers. *Heliyon* **9**(1), e12873 (2023).
36. Huang, Z. et al. PTPN2 regulates the activation of KRAS and plays a critical role in proliferation and survival of KRAS-driven cancer cells. *J. Biol. Chem.* **295**(52), 18343–18354 (2020).
37. Guo, X., Huang, X. & Chen, M. J. Reversible phosphorylation of the 26S proteasome. *Protein Cell* **8**(4), 255–272 (2017).
38. Hunter, T. The genesis of tyrosine phosphorylation. *Cold Spring Harb. Perspect. Biol.* **6**(5), a020644 (2014).
39. Chen, L. et al. Proteasome regulation by reversible tyrosine phosphorylation at the membrane. *Oncogene* **40**(11), 1942–1956 (2021).
40. Bettaieb, A. et al. Differential regulation of endoplasmic reticulum stress by protein tyrosine phosphatase 1B and T cell protein tyrosine phosphatase. *J. Biol. Chem.* **286**(11), 9225–9235 (2011).
41. Elvira, B. et al. PTPN2 regulates the interferon signaling and endoplasmic reticulum stress response in pancreatic  $\beta$ -cells in autoimmune diabetes. *Diabetes* **71**(4), 653–668 (2022).
42. Osowski, C. M. & Urano, F. Measuring ER stress and the unfolded protein response using mammalian tissue culture system. *Methods Enzymol.* **490**, 71–92 (2011).
43. Li, C.-W. et al. Eradication of triple-negative breast cancer cells by targeting glycosylated PD-L1. *Cancer Cell* **33**(2), 187 (2018).
44. Papaioannou, A. et al. Stress-induced tyrosine phosphorylation of RtcB modulates IRE1 activity and signaling outputs. *Life Sci. Alliance* **5**(5), e202201379 (2022).
45. Breitwieser, G. E. Calcium sensing receptors and calcium oscillations: calcium as a first messenger. *Curr. Top. Dev. Biol.* **73**, 85 (2006).
46. Pörn-Ares, M. I., Ares, M. P. & Orrenius, S. Calcium signalling and the regulation of apoptosis. *Toxicol. In Vitro* **12**(5), 539–543 (1998).
47. Csordás, G., Thomas, A. P. & Hajnóczky, G. Quasi-synaptic calcium signal transmission between endoplasmic reticulum and mitochondria. *EMBO J.* **18**(1), 96 (1999).
48. Lindner, P., Christensen, S. B., Nissen, P., Möller, J. V. & Engedal, N. Cell death induced by the ER stressor thapsigargin involves death receptor 5, a non-autophagic function of MAP1LC3B, and distinct contributions from unfolded protein response components. *Cell Commun. Signal* **18**(1), 12 (2020).
49. Brown, M. et al. An initial phase of JNK activation inhibits cell death early in the endoplasmic reticulum stress response. *J. Cell Sci.* **129**(12), 2317–2328 (2016).
50. Li, Y., Guo, Y., Tang, J., Jiang, J. & Chen, Z. New insights into the roles of CHOP-induced apoptosis in ER stress. *Acta Biochim. Biophys. Sin. (Shanghai)* **46**(8), 629–640 (2014).
51. Liu, Z., Lv, Y., Zhao, N., Guan, G. & Wang, J. Protein kinase R-like ER kinase and its role in endoplasmic reticulum stress-decided cell fate. *Cell Death Dis.* **6**(7), e1822–e1822 (2015).
52. Perea, V. et al. PERK signaling promotes mitochondrial elongation by remodeling membrane phosphatidic acid. *EMBO J.* **42**(15), e113908 (2023).
53. Brar, K. K., Hughes, D. T., Morris, J. L., Subramanian, K., Krishna, S., Gao, F., Rieder, L. -S., Uhrig, S., Freeman, J. & Smith, H. L. et al. PERK-ATAD3A interaction provides a subcellular safe haven for protein synthesis during ER stress. *Science*, **0**(0): eadp7114.
54. Avivar-Valderas, A. et al. Regulation of autophagy during ECM detachment is linked to a selective inhibition of mTORC1 by PERK. *Oncogene* **32**(41), 4932–4940 (2013).
55. Aradi, B. et al. Protein tyrosine phosphatase nonreceptor type 2: An important regulator of Interleukin-6 production in rheumatoid arthritis synovial fibroblasts. *Arthritis Rheumatol.* **67**(10), 2624–2633 (2015).
56. Jiang, Q. et al. Involvement of p38 in signal switching from autophagy to apoptosis via the PERK/eIF2 $\alpha$ /ATF4 axis in selenite-treated NB4 cells. *Cell Death Dis.* **5**(5), e1270 (2014).
57. Wang, C. et al. Thapsigargin induces apoptosis when autophagy is inhibited in HepG2 cells and both processes are regulated by ROS-dependent pathway. *Environ. Toxicol. Pharmacol.* **41**, 167–179 (2016).

58. Zhang, S. et al. Inhibition of autophagy promotes caspase-mediated apoptosis by tunicamycin in HepG2 cells. *Toxicol. Mech. Methods* **24**(9), 654–665 (2014).

## Acknowledgements

The author would like to thank the scientific research platform provided by Nankai University School of Medicine and the support of the National Natural Science Foundation of China (No. 81872325) and Tianjin Research Program of Application Foundation and Advanced Technology (No. 20JCYBJC01500). We thank the associate editor and the reviewers for their useful feedback that improved this paper.

## Author contributions

Na Luo: Project administration, Supervision, Funding acquisition, Writing—Review & Editing; Yanhe An: Conceptualization, Methodology, Formal analysis, Investigation, Data Curation, Writing—Original Draft, Visualization; Jinxin Lan: Methodology; Formal analysis; Writing—Review & Editing, Resources; Jiaping Tang: Validation, Resources, Software.

## Funding

This study was supported by the National Natural Science Foundation of China (No. 81872325), Tianjin Research Program of Application Foundation and Advanced Technology (No. 20JCYBJC01500).

## Declarations

## Competing interest

The authors declare no competing interests.

## Additional information

**Supplementary Information** The online version contains supplementary material available at <https://doi.org/10.1038/s41598-025-04312-w>.

**Correspondence** and requests for materials should be addressed to N.L.

**Reprints and permissions information** is available at [www.nature.com/reprints](http://www.nature.com/reprints).

**Publisher's note** Springer Nature remains neutral with regard to jurisdictional claims in published maps and institutional affiliations.

**Open Access** This article is licensed under a Creative Commons Attribution-NonCommercial-NoDerivatives 4.0 International License, which permits any non-commercial use, sharing, distribution and reproduction in any medium or format, as long as you give appropriate credit to the original author(s) and the source, provide a link to the Creative Commons licence, and indicate if you modified the licensed material. You do not have permission under this licence to share adapted material derived from this article or parts of it. The images or other third party material in this article are included in the article's Creative Commons licence, unless indicated otherwise in a credit line to the material. If material is not included in the article's Creative Commons licence and your intended use is not permitted by statutory regulation or exceeds the permitted use, you will need to obtain permission directly from the copyright holder. To view a copy of this licence, visit <http://creativecommons.org/licenses/by-nc-nd/4.0/>.

© The Author(s) 2025